IET Renewable Power Generation

Research Article

Unified decentralised control for both grid-connected and islanded operation of cascaded-type microgrid

ISSN 1752-1416
Received on 8th October 2019
Revised 23rd July 2020
Accepted on 14th August 2020
doi: 10.1049/iet-rpg.2019.0990
www.ietdl.org

Lang Li[1], Yao Sun[1] ✉, Xiaochao Hou[2], Mei Su[1], Xin Zhang[3], Peng Wang[3], Josep M. Guerrero[4]
[1]School of Automation, Central South University, Changsha 410083, People's Republic of China
[2]Department of Electrical Engineering, Tsinghua University, Beijing 100084, People's Republic of China
[3]School of Electrical and Electronic Engineering, Nanyang Technological University, Singapore 639798, Singapore
[4]Department of Energy Technology, Aalborg University, DK-9220 Aalborg East, Denmark
✉ *E-mail: yaosuncsu@gmail.com*

Abstract: In order to ensure the uninterrupted power supply, it is necessary for the microgrid to operate in both grid-connected mode and islanded mode. To address this concern, this study proposes a unified decentralised control strategy for both grid-connected and islanded operation of the cascaded-type microgrid (CMG). It can realise the smooth mode switching without the need of changing controllers. In terms of the proposed scheme, the system always holds a unique equilibrium point regardless of the grid-connected or islanded operation. Since the CMG is performed in a decentralised manner without any communication, it is a reliable and cost-effective solution. Moreover, the self-synchronisation of each DG is obtained under both the resistance–inductance (RL) and resistance–capacitance (RC) loads. The small-signal stability is proved and the design of control parameters is given. Finally, the feasibility of the proposed method is verified by simulation and OPAL-RT-based real-time simulation results.

1 Introduction

With the development of social economy and technology, the demand for electrical energy is increasing rapidly [1]. In addition, the use of conventional fossil fuels is decreased due to environmental and political restrictions [2]. This leads to the increasing use of distributed generations (DGs) [3, 4]. These DGs are conducted with microgrid implementation [5, 6]. The concept of a microgrid is firstly proposed in 2002 by Lasseter [7]. It could integrate DGs, energy storages and loads into the modern power distribution system to maintain a high level of service and reliability [8–10].

The microgrid, based on the paralleled inverters, is a low-voltage grid, which needs expensive and bulky step-up transformers to form a higher voltage level power system network [11, 12]. On the contrary, the cascaded H-bridge inverters have the potential advantage of developing medium-/high-voltage level power network conveniently [13–16]. They are earlier used to the multilevel inverters [17], AC-stacked PV systems [18, 19], battery Q1 energy storage systems [20], and gradually expanded to cascaded-type microgrid (CMG) applications [21]. For the CMG, it has been attracted an increasing research interest on the coordinated control of DGs [22].

In the grid-connected mode, Yu *et al.* [23], Chatzinikolaou and Rogers [24], Malinowski *et al.* [11] have been conducted abundant Q2 researches about the centralised control schemes. However, the implementation of these methods is highly dependent on the high bandwidth communications and centralised controller to gather global information. It will lead to reduced reliability due to communication failure and higher capital costs. Further, He *et al.* [25] introduced a proper power-sharing control scheme, in which the low bandwidth communication links are necessary. Although the communication-based methods hold excellent power sharing and voltage quality, it is sensitive to the single-point failure. Then, Hou *et al.* [26] proposed a decentralised control scheme of CMG in the grid-connected mode. This method has the advantages of improved reliability and decreased capital costs. However, it is unable to be used in the islanded mode directly.

Q3 In the islanded mode, Mortezaei *et al.* [21] introduced the single-loop and multi-loop voltage control schemes of the CMG. This method does not need any current measurement; however, the communication networks are required. Further, He *et al.* [27] proposed an inverse power factor droop control strategy for accurate power sharing. Although this method is a fully decentralised one, it is unfeasible to feed the resistance–Q4 capacitance (RC) loads. To broaden this limitation, Sun *et al.* [28] presented an *f-P/Q* control method, which can be fed by both the resistance–inductance (RL) and RC loads. This method can share the active and reactive power accurately; nevertheless, it has the problem of multiple equilibrium points. This problem may bring about some undesired operating states. Then, Li *et al.* [29] introduced a decentralised control with a unique equilibrium point, which can solve the limitation in [28] and realise the self-synchronised operation. However, it cannot be directly apply to the grid-connected operation mode of CMG.

It is necessary for CMG to work in two modes, i.e. grid-connected mode and islanded mode [30–32]. However, the existing decentralised control methods can only be applied to grid-connected or islanded operation. They cannot directly be used as a unified decentralised control in these two operation modes of CMG. To overcome the limitation, this paper proposes a unified decentralised control strategy of CMG for both the grid-connected and islanded operation. Its main features are summarised as follows:

(i) both the grid-connected and islanded operation are realised with a unified controller;
(ii) seamless transition from the grid-connected mode to islanded mode is obtained;
(iii) the decentralised manner with a unique equilibrium point is realised;
(iv) the synchronisation is achieved under both the RL and RC loads.

The rest of the paper is organised as follows. Section 2 introduces the equivalent models of the CMG and their typical control strategies. The proposed unified decentralised control scheme for both grid-connected and islanded operation mode is presented in Section 3. The steady-state analysis and small-signal stability analysis of the system are introduced in Section 4. Then, the

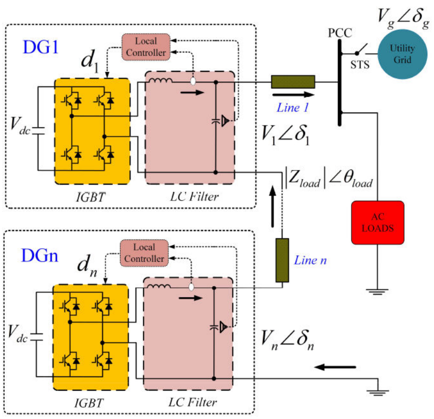

Fig. 1 *Structure of the CMG*

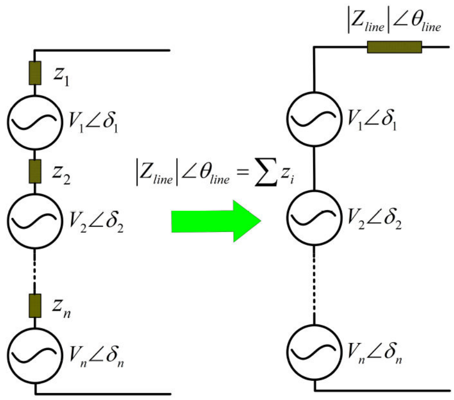

Fig. 2 *Equivalent circuit of the series DGs*

simulation validations in Section 5 and OPAL-RT-based real-time simulation tests in Section 6 are presented to verify the effectiveness of the proposed scheme. Finally this paper is concluded in Section 7.

2 Equivalent models of CMG and its control

2.1 Equivalent models of CMG

The structure of the CMG consisting of n DG units is shown in Fig. 1 [21, 22]. The CMG can operate in the grid-connected or islanded mode by switching the static transfer switch (STS). z_i is the line impedance. The equivalent circuit of the series DGs is shown in Fig. 2. $|Z_{\rm line}|\angle\theta_{\rm line}$ is the generalised transmission impedance, $|Z_{\rm line}|\angle\theta_{\rm line} = \sum z_i$. In both medium- and high-voltage systems, the line impedance is mainly inductive, i.e. $\theta_{\rm line} \simeq \pi/2$.

In the islanded mode, the output active power P_i and reactive power Q_i of the ith DG are derived as follows:

$$P_i + \mathrm{j}Q_i = V_i \mathrm{e}^{\mathrm{j}\delta_i}\left(\sum_{i=1}^{n} V_i \mathrm{e}^{\mathrm{j}\delta_i}/|Z'_{\rm load}|\mathrm{e}^{\mathrm{j}\theta'_{\rm load}}\right)^* \tag{1}$$

where V_i and δ_i represent the voltage and phase angle of the ith unit, respectively. $Z'_{\rm load}$ and $\theta'_{\rm load}$ are the impedance and impedance angle of the generalised load, which include the generalised transmission line and load, respectively. Then, the power transmission characteristic in the islanded mode is given by

$$P_i = \frac{V_i}{|Z'_{\rm load}|}\sum_{j=1}^{n} V_j \cos(\delta_i - \delta_j + \theta'_{\rm load}) \tag{2}$$

$$Q_i = \frac{V_i}{|Z'_{\rm load}|}\sum_{j=1}^{n} V_j sin(\delta_i - \delta_j + \theta'_{\rm load}) \tag{3}$$

When the output voltages V_i and V_j are set to be constant, the active power and reactive power regulations are mainly related to $\theta'_{\rm load}$ in the islanded mode.

In the grid-connected mode, P_i and Q_i are expressed as

$$P_i + \mathrm{j}Q_i = V_i \mathrm{e}^{\mathrm{j}\delta_i}\left(\left(\sum_{i=1}^{n} V_i \mathrm{e}^{\mathrm{j}\delta_i} - V_{\rm g}\mathrm{e}^{\mathrm{j}\delta_{\rm g}}\right)/|Z_{\rm line}|\mathrm{e}^{\mathrm{j}\theta_{\rm line}}\right)^* \tag{4}$$

where $V_{\rm g}$ and $\delta_{\rm g}$ represent the voltage amplitude and phase angle of the grid, respectively. The power transmission characteristic in the grid-connected mode is

$$P_i = \frac{V_i}{|Z_{\rm line}|}\left(V_{\rm g}\sin(\delta_i - \delta_{\rm g}) - \sum_{j=1}^{n} V_j \sin(\delta_i - \delta_j)\right) \tag{5}$$

$$Q_i = \frac{V_i}{|Z_{\rm line}|}\left(\sum_{j=1}^{n} V_j \cos(\delta_i - \delta_j) - V_{\rm g}\cos(\delta_i - \delta_{\rm g})\right) \tag{6}$$

As seen, the active power and reactive power could be regulated by the output voltage and the phase angle differences in the grid-connected mode.

2.2 Review of the typical control schemes

In the islanded mode, the decentralised control scheme is introduced in [29]:

Q5

$$\omega_i = \omega^* + m\mathrm{sgn}(Q_i)P_i \tag{7}$$

$$\boldsymbol{v}_i = \begin{cases} V^* sin\left(\int \omega_i \mathrm{d}t\right), & P_i \geq 0 \\ V^* sin\left(\int \omega_i \mathrm{d}t + \pi\right), & P_i < 0 \end{cases} \tag{8}$$

where ω_i, ω^*, and V^* are the angular frequency, the nominal angular frequency and voltage amplitude, respectively. $\boldsymbol{v}_i$ is the voltage vector. m is a positive coefficient. sgn() is a signum function:

$$\mathrm{sgn}(x) = \begin{cases} 1, & x > 0 \\ 0, & x = 0 \\ -1, & x < 0 \end{cases} \tag{9}$$

In (7), the adverse droop control is applied to feeding the RL load ($Q_i > 0$), while the droop control is for the RC load ($Q_i < 0$). Equation (8) is to achieve the unique equilibrium point.

In the grid-connected mode, the decentralised control scheme in [26] is expressed as

$$\begin{cases} \omega_i = \omega^* - mP_i \\ \boldsymbol{v}_i = V^* sin\left(\int \omega_i \mathrm{d}t\right) \end{cases} \tag{10}$$

The droop control is performed to realise the frequency synchronisation of the system.

As seen, the adverse droop and droop control are applied in the islanded mode, and the droop control is used in the grid-connected mode. However, the methods in [26, 29] cannot be served as a unified control scheme for the two modes under the RL and RC loads.

3 Proposed unified decentralised control

The proposed unified decentralised control strategy for grid-connected and islanded operation of the CMG is expressed as

$$\omega_i = \omega^* + m\mathrm{sgn}(Q_i)\mathrm{sgn}(P_i)P_i \tag{11}$$

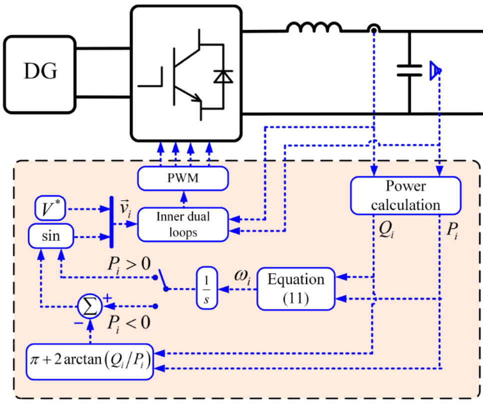

Fig. 3 *Control diagram of the ith DG*

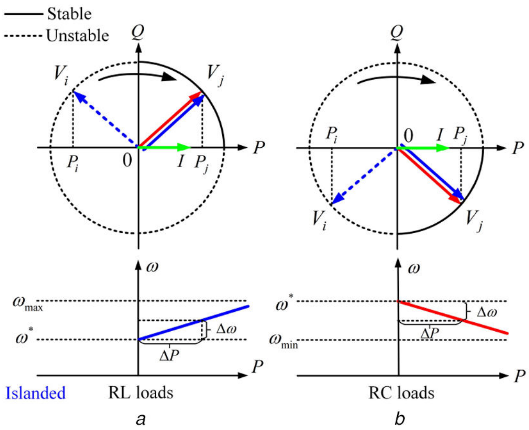

Fig. 4 *Schematic of the uniqueness of steady-state operation point in the islanded mode*
(a) RL loads, ***(b)*** RC loads

$$\boldsymbol{v}_i = \begin{cases} V^* \sin\left(\int \omega_i \mathrm{d}t\right), P_i \geq 0 \\ V^* \sin\left(\int \omega_i \mathrm{d}t - (\pi + 2\arctan(Q_i/P_i))\right), P_i < 0 \end{cases} \tag{12}$$

Equation (12) is applied to guarantee the unique equilibrium point of the system. The output voltage of the ith DG is regulated to track $\boldsymbol{v}_i$ through the inner dual-loop controller [33–35], and its control diagram is depicted in Fig. 3.

The control parameters in (11) and (12) are given as (13), which will be illustrated in Section 4 detailedly:

$$\begin{cases} 0 < m < (\omega_{\max} - \omega_{\min})/2P_{\text{Rated}} \\ \omega_g < \omega^* < \omega_{\max} \\ \varepsilon V_g/n \leq V^* < \cos\bar{\delta} V_g/n \end{cases} \tag{13}$$

where P_{Rated} is the rated active power, and $\omega_{\max}$ and $\omega_{\min}$ are the allowable maximum and minimum angular frequencies of CMG, respectively. ε is designed to ensure the load voltage quality (higher than its allowable minimum values in the islanded mode), which is set at 0.95 in this paper. The selecting of V^* is the tradeoff between the system stability and load voltage quality.

Compared to the method in [29], the terms $\mathrm{sgn}(P_i)$ and $\omega^* > \omega_g$ are performed to make the system work in the 'droop'. Then, it is applied to the grid-connected mode. Thus, the unified control for the two modes is realised. Clearly, the proposed scheme (11) and (12) can be implemented with only local information, thus it is a decentralised control.

4 Stability analysis

In this section, the small-signal stability near the steady-state operating point of the CMG will be investigated.

4.1 Steady-state analysis

When the system is in the steady state, according to (11), we have

$$\mathrm{sgn}(Q_i)|P_i| = \mathrm{sgn}(Q_j)|P_j|, \ i \neq j \tag{14}$$

As the output voltage amplitude and current of all DG units are the same, i.e. $V_i = V_j = V^*$ and $I_i = I_j$, (15) is satisfied:

$$|P_i + \mathrm{j}Q_i| = |P_j + \mathrm{j}Q_j| \tag{15}$$

Combine (14) and (15), if $|P_i| \neq 0$ and $|Q_i| \neq 0$, then

$$\begin{cases} P_i = P_j \text{ or } P_i = -P_j \\ Q_i = Q_j \end{cases} \tag{16}$$

Thus, the reactive power can be shared accurately in CMG.

In the islanded mode, the undesired steady-state $P_i = -P_j$ is removed through (12), which has been explained in [29], its detail is omitted here. The system always holds a unique equilibrium point $Q_i = Q_j$ and $P_i = P_j$ when feeding both RL and RC loads, which is depicted in Figs. 4*a* and *b*, respectively. In other words, $(\delta_i - \delta_j) = 0$ is always achieved in the steady state. From (2) and (3), we have

$$P_i = n(V^*)^2 \cos\theta'_{\text{load}}/|Z'_{\text{load}}| \tag{17}$$

$$Q_i = n(V^*)^2 \sin\theta'_{\text{load}}/|Z'_{\text{load}}| \tag{18}$$

Assume that the reactive power losses of transmission line can be neglected. Since the active and reactive power land demands $\sum P_i = P_{\text{load}}$ and $\sum Q_i = Q_{\text{load}}$, then the unique steady-state operating point is expressed as

$$\begin{cases} P_i = P_j = P_{\text{load}}/n \\ Q_i = Q_j = Q_{\text{load}}/n \end{cases} \tag{19}$$

In the grid-connected mode, assume that ω_g is the identical grid angular frequency, there is $\omega_i = \omega_g$. Equation (11) can be rewritten as

$$\mathrm{sgn}(P_i)P_i = \mathrm{sgn}(P_j)P_j = (\omega_g - \omega^*)/m\,\mathrm{sgn}(Q_i) = \bar{P}^* \tag{20}$$

There is $\mathrm{sgn}(P_i)P_i = \mathrm{sgn}(P_j)P_j = \bar{P}^* > 0$.

Similarly, the unique equilibrium points $Q_i = Q_j$ and $P_i = P_j = \bar{P}^*$ are obtained, which is depicted in Fig. 5.

Assume $\bar{\delta} = \delta_i - \delta_g$ in the steady state, from (5) and (6), we have

$$P_i = V^* V_g \sin\bar{\delta}/|Z_{\text{line}}| \tag{21}$$

$$Q_i = V^*\left(nV^* - V_g \cos\bar{\delta}\right)/|Z_{\text{line}}| \tag{22}$$

As $\omega^* > \omega_g$, it can be deduced from (20) that $Q_i < 0$. Combine (22), then

$$nV^* - V_g \cos\bar{\delta} < 0 \tag{23}$$

Thus, $V^* < \cos\bar{\delta} V_g/n$ holds in (13). Then $\cos\bar{\delta} > 0$ and $\bar{\delta} \in (-\pi/2, \pi/2)$. Combining $P_i = P_j = \bar{P}^*$, the obtained steady-state operating point of the system is $\bar{\delta} \in (0, \pi/2)$, i.e. $\bar{\delta} = \arcsin\left(\bar{P}^* |Z_{\text{line}}|/V^* V_g\right)$.

Based on the analysis above, the active power and reactive power can be shared accurately in both islanded and grid-connected modes. In addition, the characteristics of the proposed control scheme (11) and (12) are summarised in Table 1, which is depicted in Figs. 4 and 5.

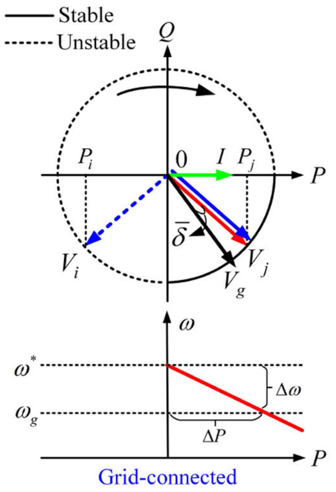

Fig. 5 *Schematic of the uniqueness of steady-state operation point in the grid-connected mode*

Table 1 Characteristics of the proposed strategy

Operation mode	Load	Characteristic
islanded mode	RL load	adverse droop control
	RC load	droop control
grid-connected mode	RL and RC loads	droop control

4.2 Small-signal stability analysis

For the decentralised control, each DG makes decisions only based on their local information. Thus, the self-synchronisation of phase angles is the most essential and crucial problem. Suppose that the inner voltage and current control loops can track the given reference voltage without the steady-state error.

In the islanded mode, assume δ_s is the steady-state synchronised phase angle and denote $\tilde{\delta}_i = \delta_i - \delta_s$, $\dot{\tilde{\delta}}_i = \omega_i$. Linearising (2) and (11) near the equilibrium point (19), we have

$$\Delta P_i = -\frac{(V^*)^2}{|Z'_{\text{load}}|}\sin(\theta'_{\text{load}})\sum_{j=1}^{n}\left(\Delta\tilde{\delta}_i - \Delta\tilde{\delta}_j\right) \tag{24}$$

$$\Delta\dot{\tilde{\delta}}_i = m\,\text{sgn}(Q_{\text{load}}/n)\Delta P_i \tag{25}$$

Substituting (24) into (25) yields

$$\Delta\dot{\tilde{\delta}}_i = -m\,\text{sgn}(Q_{\text{load}}/n)(V^*)^2\sin(\theta'_{\text{load}})\sum_{j=1}^{n}\left(\Delta\tilde{\delta}_i - \Delta\tilde{\delta}_j\right)/|Z'_{\text{load}} \tag{26}$$

|

Rewriting (26) in the matrix form

$$\dot{\boldsymbol{X}} = \boldsymbol{A}\boldsymbol{X} \tag{27}$$

where

$$\boldsymbol{X} = \left[\Delta\tilde{\delta}_1 \quad \cdots \quad \Delta\tilde{\delta}_n\right]^{\text{T}} \tag{28}$$

$$\boldsymbol{A} = -K_1\left(n\boldsymbol{I}_{n\times n} - \boldsymbol{1}_n\boldsymbol{1}_n^{\text{T}}\right) \tag{29}$$

$$K_1 = m\,\text{sgn}(Q_{\text{load}}/n)(V^*)^2\sin(\theta'_{\text{load}})/|Z'_{\text{load}}| \tag{30}$$

From (29), the eigenvalues of $\boldsymbol{A}$ are expressed as

$$\lambda_1(\boldsymbol{A}) = 0, \lambda_2(\boldsymbol{A}) = \cdots = \lambda_n(\boldsymbol{A}) = -nK_1 \tag{31}$$

There is one zero eigenvalue, which is corresponding to rotational invariance of the dynamics as explained in [36]. As seen, $m > 0$ [see (13)], in case of RL or RC loads, $K_1 > 0$, thus, the system is stable. Therefore, the proposed scheme is feasible for the islanded operation under RL and RC loads. If $\theta'_{\text{load}} = 0$ ($Q_i = 0$) or under no-load condition ($P_i = 0$ and $Q_i = 0$), from (11), $\omega_i = \omega^*$, the system operates in constant frequency and it is stable.

In the grid-connected mode, similarly, linearising (5) and (11) near the equilibrium point yields

$$\Delta P_i = \frac{V^*}{|Z_{\text{line}}|}\left(V_{\text{g}}\cos\bar{\delta}\Delta\tilde{\delta}_i - V^*\sum_{j=1}^{n}\left(\Delta\tilde{\delta}_i - \Delta\tilde{\delta}_j\right)\right) \tag{32}$$

$$\Delta\dot{\tilde{\delta}}_i = -m\Delta P_i \tag{33}$$

Substituting (32) into (33), we have

$$\Delta\dot{\tilde{\delta}}_i = -mV^*(V_{\text{g}}\cos\bar{\delta}\Delta\tilde{\delta}_i - V^*\sum_{j=1}^{n}\left(\Delta\tilde{\delta}_i - \Delta\tilde{\delta}_j\right))/|Z_{\text{line}}| \tag{34}$$

Rewrite (34) in the matrix form as (35):

$$\dot{\boldsymbol{X}} = \bar{\boldsymbol{A}}\boldsymbol{X} \tag{35}$$

where

$$\bar{\boldsymbol{A}} = K_2\left(\left(V_{\text{g}}\cos\bar{\delta} - nV^*\right)\boldsymbol{I}_{n\times n} + V^*\boldsymbol{1}_n\boldsymbol{1}_n^{\text{T}}\right) \tag{36}$$

$$K_2 = -mV^*/|Z_{\text{line}}| < 0 \tag{37}$$

The eigenvalues of the system matrix $\bar{\boldsymbol{A}}$ are given as follows:

$$\lambda_1\left(\bar{\boldsymbol{A}}\right) = K_2V_{\text{g}}\cos\bar{\delta}, \lambda_2\left(\bar{\boldsymbol{A}}\right) = \cdots = \lambda_n\left(\bar{\boldsymbol{A}}\right) = K_2\left(V_{\text{g}}\cos\bar{\delta} - nV^*\right) \tag{38}$$

Since $\left(V_{\text{g}}\cos\bar{\delta} - nV^*\right) > 0$ [see (13)], $\cos\bar{\delta} > 0$ and $|Z_{\text{line}}| > 0$, the system is stable according to (38). As $V_{\text{g}} \geq V_{\text{g}}\cos\bar{\delta}$, then $V_{\text{g}} > nV^*$, that is to say $Q_i < 0$ is needed for the requirement of stable operation. Thus, the system is also feasible for the grid-connected operation.

From the above theoretical analysis, the proposed unified decentralised control is stable under both the grid-connected and islanded mode while the control parameters (13) and line impedance $|Z_{\text{line}}| > 0$ satisfied. Thus, the seamless transition from grid-connected mode to islanded mode of CMG is obtained via the decentralised manner.

Furthermore, as the expansion of main idea in this paper, for the active synchronisation from the islanded mode to the grid-connected mode, we can modify (11) as

$$\omega_i = \omega^* + m\,\text{sgn}(Q_i)\text{sgn}(P_i)P_i + \Delta\omega_i \tag{39}$$

$$\Delta\omega_i = k_w\int\left(\omega_{\text{g}} - \omega_i\right)\text{d}t \tag{40}$$

where k_w is a positive constant. $\Delta\omega_i$ is the compensation signal, and it is enabled when the CMG needs to switch from the islanded mode to the grid-connected mode.

5 Simulation results

The proposed unified decentralised control strategy is verified on MATLAB/Simulink platform. This simulation model of CMG comprises four DGs, which is shown in Fig. 6. The associated parameters are listed in Table 2.

5.1 Case 1: islanded mode under RL and RC loads

This case is performed to test the effectiveness of the proposed scheme in the islanded mode. The load demands are shown in

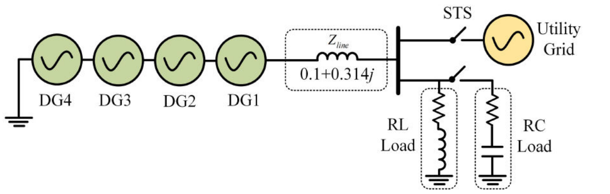

Fig. 6 *Simulation model of a CMG*

Table 2 Parameters for simulations

Item	Symbol	Value	Unit
line inductance	L_{line}	1×10^{-3}	H
line resistance	R_{line}	0.1	Ω
filter inductance	L_f	1.5×10^{-3}	H
resistance in filter inductance	r_f	0.1	Ω
filter capacitor	C_f	20	μF
resistance in filter capacitor	r_d	3.3	Ω
voltage reference	V^*	77.13	V
nominal grid frequency	f_g	50	Hz
allowable load voltage ranges	V_{pcc}	[295.45, 326.55]	V
frequency reference	f^*	50.2	Hz
allowable frequency ranges	f	[49,51]	Hz
sharing coefficients	m	1×10^{-4}	rad/(W s)

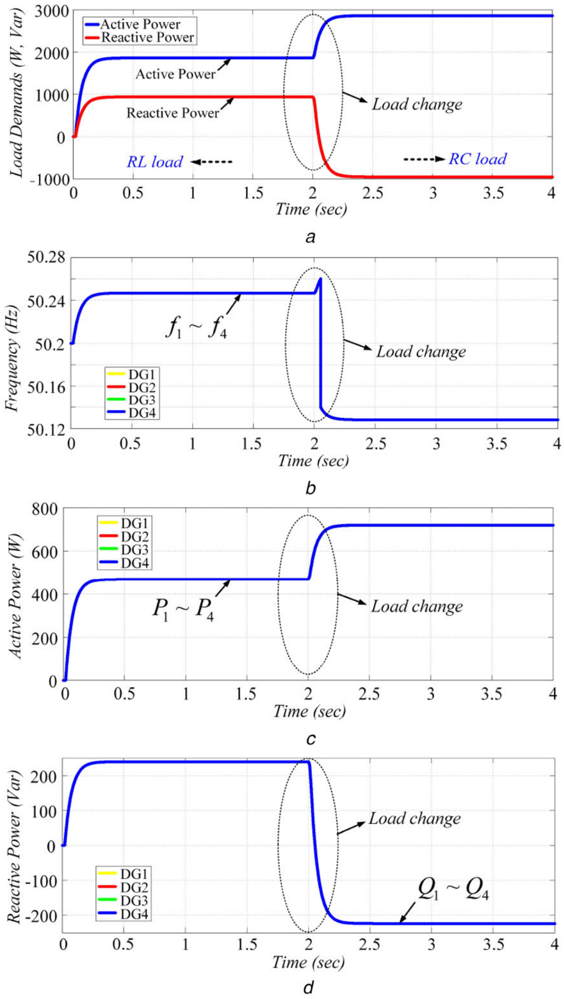

Fig. 7 *Simulation results of case 1*
(a) Load demands, ***(b)*** Frequency, ***(c)*** Active power, ***(d)*** Reactive power

Fig. 7*a*, which are fed by RL loads in the interval [0 s, 2 s] and RC loads in the interval [2 s, 4 s], respectively. The corresponding load power factors are 0.89 and 0.95. The frequencies of all DGs are

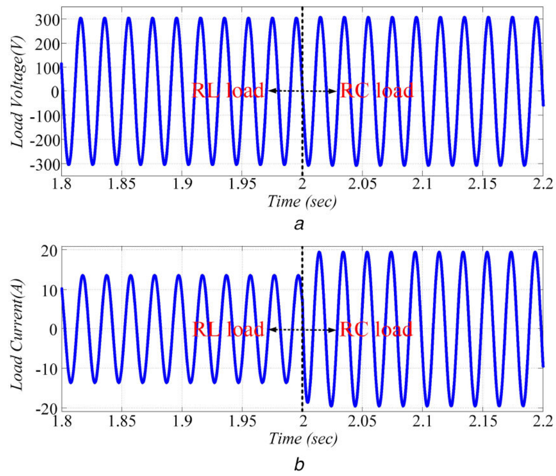

Fig. 8 *Simulation waveforms of case 1*
(a) Load voltage, ***(b)*** Load current

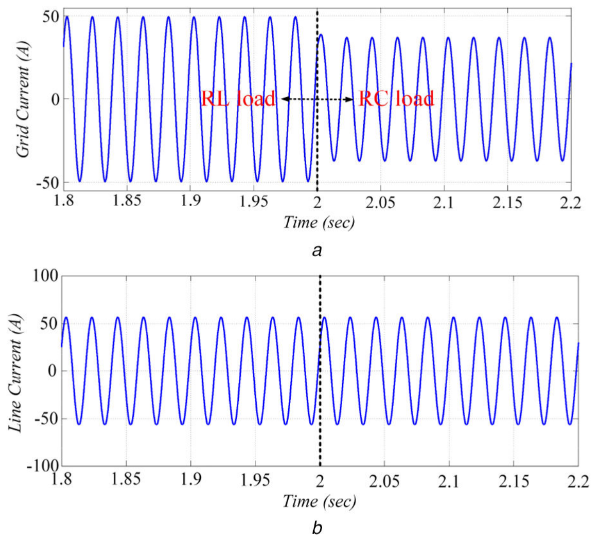

Fig. 9 *Simulation waveforms of case 2*
(a) Grid current, ***(b)*** Line current

depicted in Fig. 7*b*. As seen, all DGs can realise the self-synchronisation and maintain the system stable operation under both the RL loads and RC loads. From Fig. 7*c*, the active power allocations among DGs are always accurate. The reactive power sharing is shown in Fig. 7*d*, in which it is also accurate under the two types of loads. The load voltage and current waveforms are shown in Figs. 8*a* and *b*, in which there are some phase angle differences. From this test, the proposed scheme can realise the accurate power sharing and maintain the system stable in the islanded mode.

5.2 Case 2: grid-connected mode under RL and RC loads

In this case, the performance of the proposed scheme is verified in the grid-connected mode. The load demands are set as the same as Case 1, which is shown in Fig. 7*a*. The waveforms of grid current and line current are shown in Figs. 9*a* and *b*, respectively. The injected grid current is decreased as the active power load demands increasing, in which the power balance of system is ensured. The frequencies are shown in Fig. 10*a*, in which it converges to 50 Hz, and the proposed scheme can synchronise with the grid. The active power sharing results are depicted in Fig. 10*b*, in which the DGs can output the desired active power in the grid-connected mode. The accurate reactive power sharing is shown in Fig. 10*c*. Therefore, the proposed scheme can output the desired active power and maintain the self-synchronisation in the grid-connected mode.

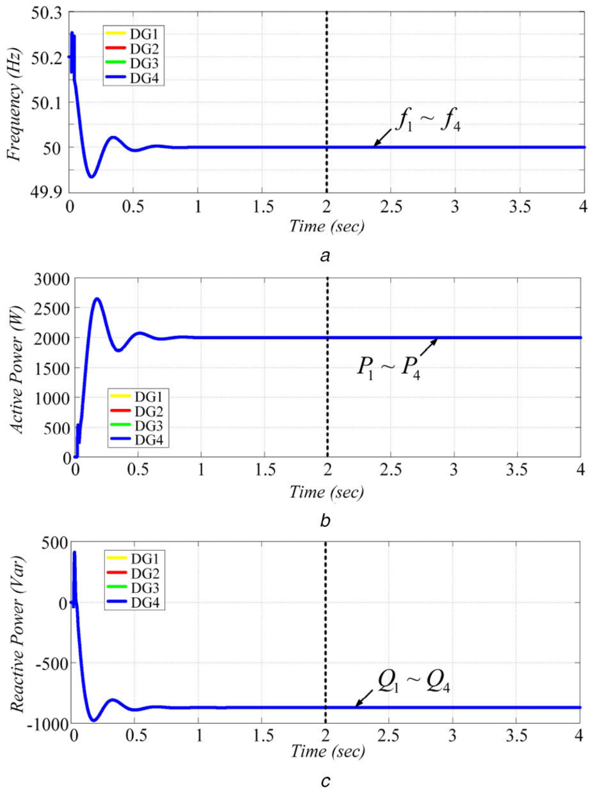

Fig. 10 *Simulation results of case 2*
(a) Frequency, ***(b)*** Active power, ***(c)*** Reactive power

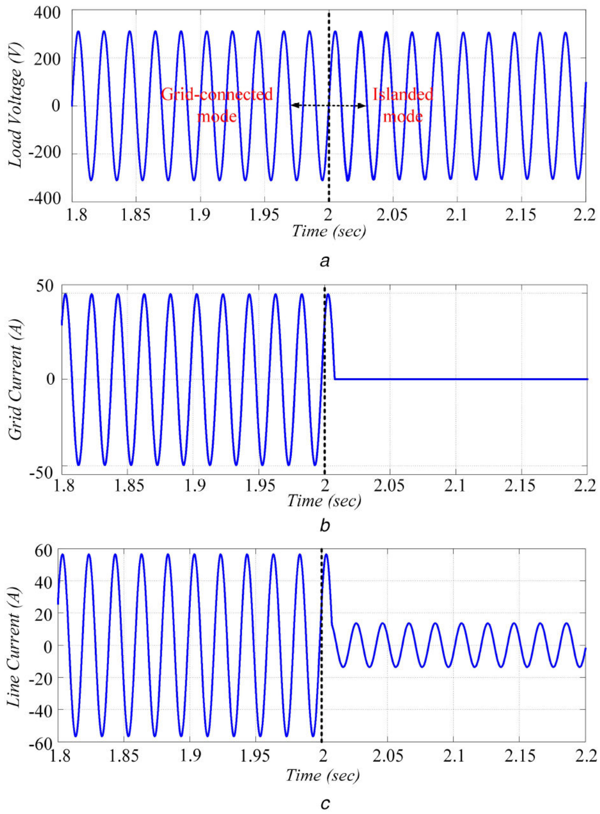

Fig. 11 *Simulation waveforms of case 3*
(a) Load voltage, ***(b)*** Grid current, ***(c)*** Line current

5.3 Case 3: switch from grid-connected to islanded mode under RL loads

This simulation is implemented during switching from the grid-connected to islanded mode under the RL loads. The load power factor is 0.89. The load voltages in the interval [1.8 s, 2.2 s] are

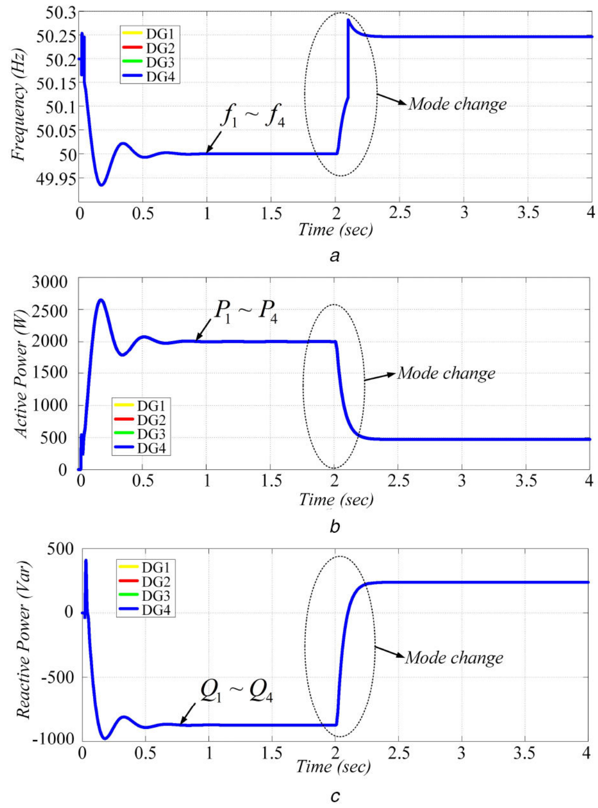

Fig. 12 *Simulation results of case 3*
(a) Frequency, ***(b)*** Active power, ***(c)*** Reactive power

shown in Fig. 11*a*, in which the sustainable power supply for the loads is obtained. The grid current and line current are shown in Figs. 11*b* and *c*, in which the waveforms are smooth while switching from the grid-connected mode to the islanded mode. The frequencies of DGs are shown in Fig. 12*a*, in which the system is always stable. The active and reactive power allocations among DGs are accurate, which are shown in Figs. 12*b* and *c*. Accordingly, it is concluded that the proposed scheme can realise the smooth operation when the system switches from the grid-connected mode to the islanded mode under the RL loads.

5.4 Case 4: switch from grid-connected to islanded mode under RC loads

This case is carried out during switching from the grid-connected to islanded mode under the RC loads. The load power factor is 0.95. The waveforms of grid current and line current are shown in Figs. 13*a* and *b*, in which the system can operate smoothly while mode switching under the RC loads. The frequencies are shown in Fig. 14*a*, in which the system is always stable. The active and reactive power allocations among DGs are depicted in Figs. 14*b* and *c*, respectively. As seen, the proposed scheme is feasible to the CMG during the mode switching from grid-connected mode to islanded mode fed by RC loads.

5.5 Case 5: performance of the proposed scheme towards removal of DG4

This test is carried out with DG4 lost at $t = 2$ s. When DG4 suddenly suffer a fault, the bypass method [37] is applied. The waveforms of active and reactive power in the islanded mode are shown in Figs. 15*a* and *b*. In the grid-connected mode, the simulation results towards the removal of DG4 are depicted in Figs. 16*a* and *b*. As seen, the CMG can realise the stable operation in both islanded and grid-connected modes. Therefore, removal of DG4 will not affect the stability of system for the proposed scheme.

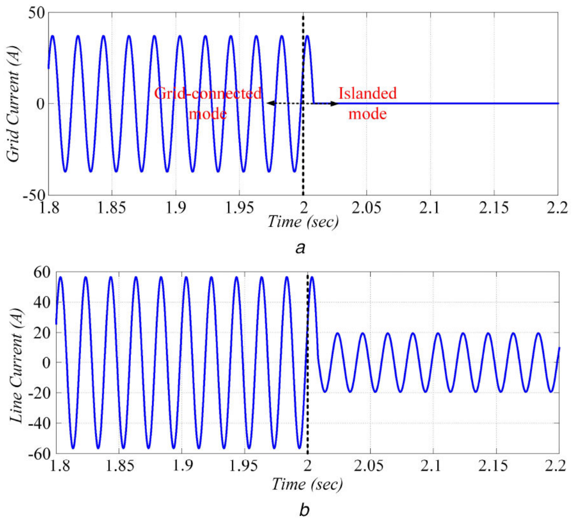

Fig. 13 *Simulation results of case 4*
(a) Grid current, ***(b)*** Line current

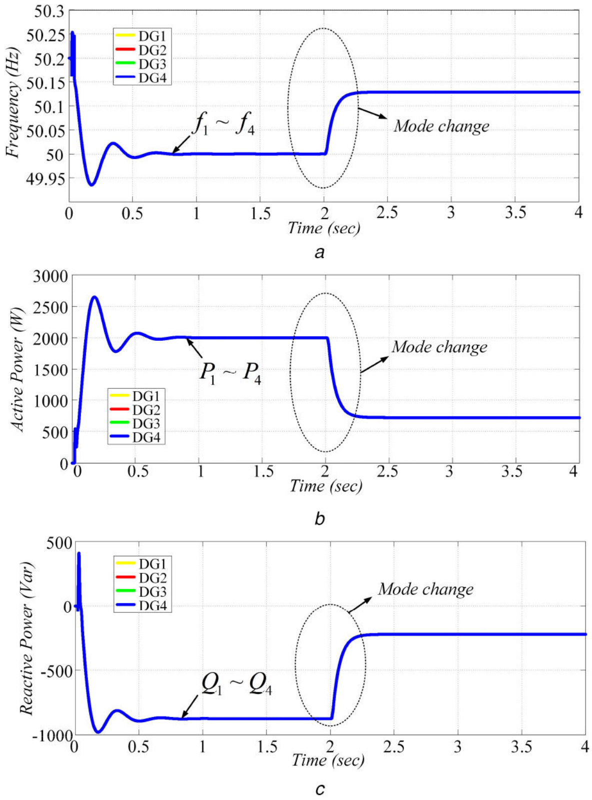

Fig. 14 *Simulation results of case 4*
(a) Frequency, ***(b)*** Active power, ***(c)*** Reactive power

5.6 Case 6: performance of the proposed scheme under single-phase asynchronous machine

This simulation is implemented to verify the performance of the proposed unified decentralised control scheme under single-phase asynchronous machine. The set mechanical torque is shown in Fig. 17*a*, which is scheduled as 0, 10, 0, 10 in the interval [0 s, 1 s], [1 s, 2 s], [2 s, 3 s], [3 s, 4 s], respectively. The CMG is switched from the grid-connected mode to islanded mode at $t = 2$ s. The speed of the single-phase asynchronous machine is shown in Fig. 17*b*. The active power and reactive power allocations are shown in Figs. 18*a* and *b*. The frequencies of DGs are presented in Fig. 18*c*. As seen, the proposed scheme is feasible for single-phase asynchronous machine load and maintains the stable operation of CMG.

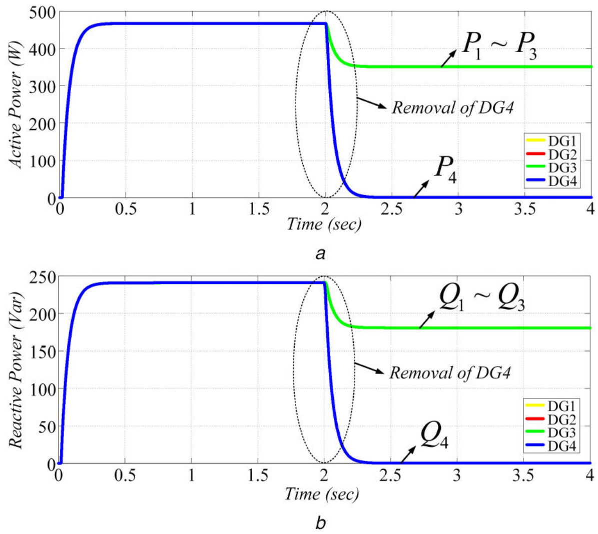

Fig. 15 *Removal of DG4 in islanded mode*
(a) Active power, ***(b)*** Reactive power

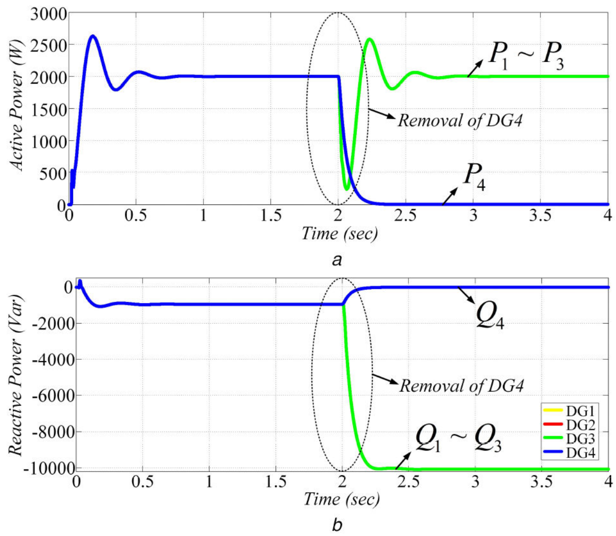

Fig. 16 *Removal of DG4 in grid-connected mode*
(a) Active power, ***(b)*** Reactive power

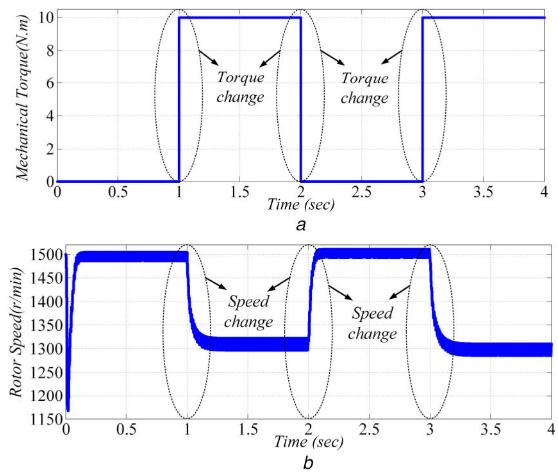

Fig. 17 *Simulation waveforms of case 6*
(a) Mechanical torque, ***(b)*** Rotor speed

5.7 Case 7: impact of line impedance

This case is carried out to investigate the impact of different line impedances in the islanded mode. The line impedance is scheduled as 1 mH (inductive) in the interval [0 s, 2 s], and 0.3 Ω (resistive) in the interval [2 s, 4 s], respectively. The simulation results are

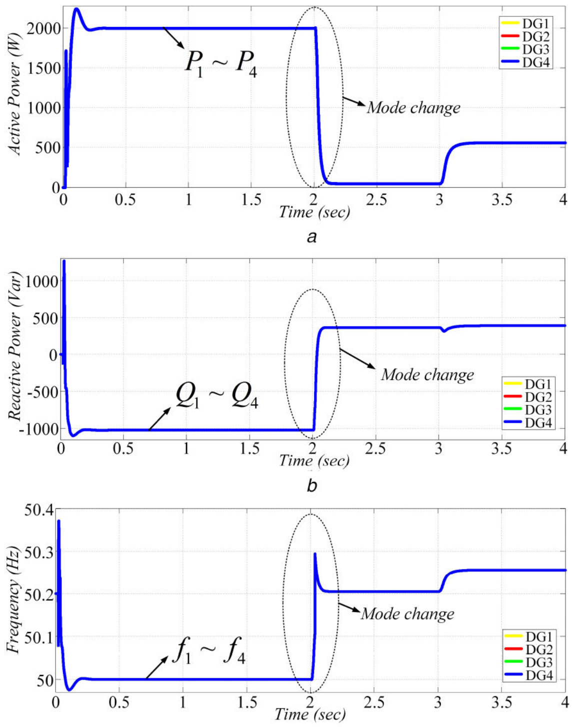

Fig. 18 *Simulation results of case 6*
(a) Active power, ***(b)*** Reactive power, ***(c)*** Frequency

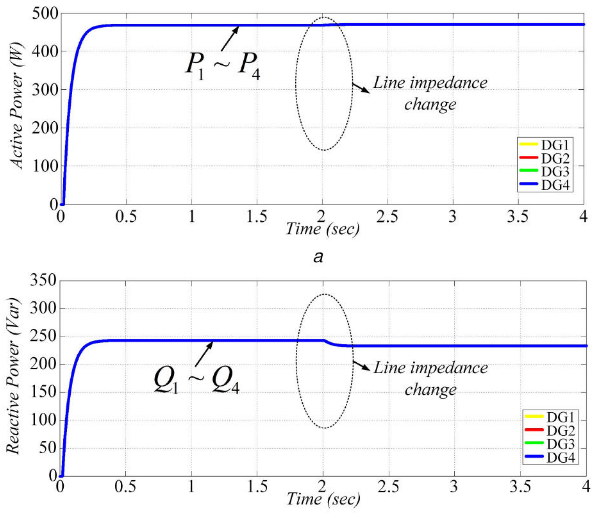

Fig. 19 *Impact of line impedance in islanded mode*
(a) Active power, ***(b)*** Reactive power

shown in Figs. 19*a* and *b*. Usually, the line impedance is much less than the load impedance, and the impact of inductive or resistive interconnecting line can be almost negligible.

5.8 Case 8: under the only resistive load or no load condition

In this case, the generalised load is set as the only resistive load in the interval [0 s, 2 s] and no load condition in the interval [2 s, 4 s], respectively. The active power and reactive power sharing are shown in Fig. 20*a*. The frequency of all DGs is shown in Fig. 20*b*, which is a constant. Therefore, under the only resistive load or no load condition, the system is stable and operates in constant frequency.

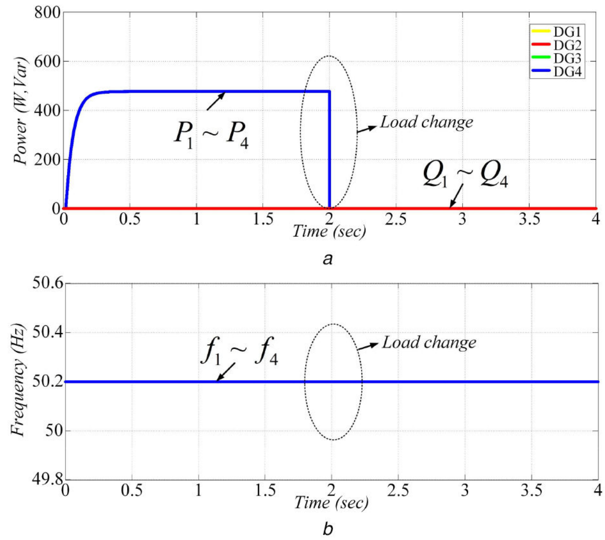

Fig. 20 *Simulation results of case 8*
(a) Power, ***(b)*** Frequency

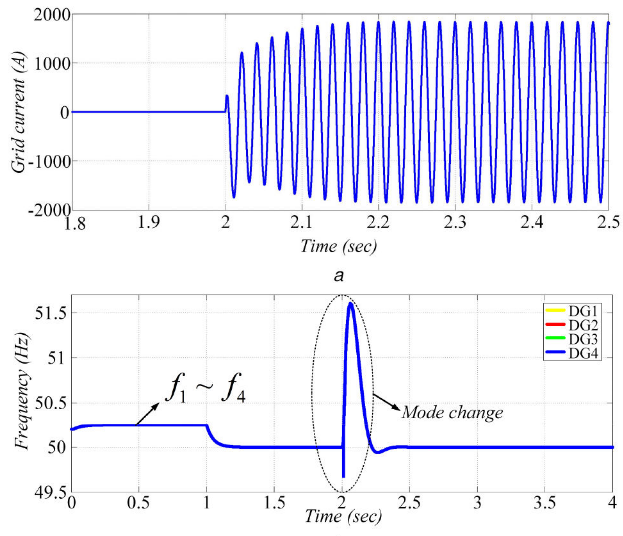

Fig. 21 *Simulation results of case 9*
(a) Grid current, ***(b)*** Frequency

5.9 Case 9: active synchronisation from the islanded mode to grid-connected mode

This case is carried out to verify the performance of active synchronisation. At $t = 1$ s, the active synchronisation control (39) is enabled, $k_w = 20$. The STS is closed at $t = 2$ s. The waveforms of grid current are shown in Fig. 21*a*, which is smooth during mode switching. The frequencies are shown in Fig. 21*b*. Accordingly, the modified active synchronisation control (39) can realise the seamless transition from the islanded mode to the grid-connected mode.

6 OPAL-RT-based real-time simulation results

The OPAL-RT-based real-time simulation tests are carried out in this section to verify the performance and effectiveness of the proposed scheme. The real-time simulation platform is based on the real-time simulator OPAL-RT 5600, whose time step is 20 µs. This considered test model is consists of four DGs, and the associated parameters are listed in Table 3.

6.1 Case 1: switch from grid-connected to islanded mode under RL loads

This test is performed when the CMG operates from the grid-connected mode to the islanded mode under the RL loads. The load

Table 3 Parameters for OPAL-RT based real-time simulation tests

Item	Symbol	Value	Unit
line inductance	L_{line}	1.5×10^{-3}	H
line resistance	R_{line}	0.1	Ω
filter inductance	L_f	0.6×10^{-3}	H
resistance in filter inductance	r_f	0.1	Ω
filter capacitor	C_f	20	μF
resistance in filter capacitor	r_d	3.3	Ω
voltage reference	V^*	308.5/4	V
nominal grid frequency	f_g	50	Hz
frequency reference	f^*	50.2	Hz
allowable frequency ranges	f	[49,51]	Hz
sharing coefficients	m	1×10^{-4}	rad/(W s)

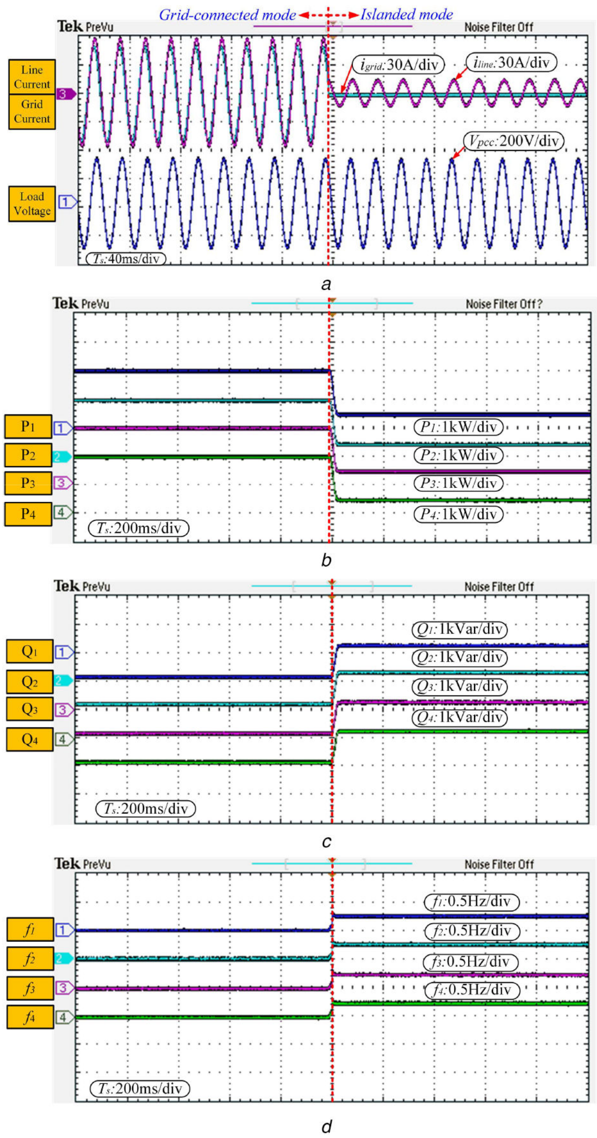

Fig. 22 *OPAL-RT-based real-time simulation tests of case 1*
(a) Voltage and current waveforms, ***(b)*** Active power, ***(c)*** Reactive power, ***(d)*** Frequency

power factor is 0.89. The waveforms of load voltage, line current and grid current are shown in Fig. 22*a*, in which the load voltage is smooth regardless of the mode change. After the mode changing, the line current reduces due to only supplying the local RL loads, and the grid current reduces to zero in the islanded mode. The active power allocations among the four DGs are shown in Fig. 22*b*. These DGs can inject the given active powers into the grid, and continuously supply electricity to the local loads. The reactive power sharing is depicted in Fig. 22*c*. The frequencies of DGs are shown in Fig. 22*d*, in which the system can always maintain the stable operation in the grid-connected and islanded modes.

Therefore, it is concluded that the proposed scheme can realise the power sharing and maintain the system table under the RL loads.

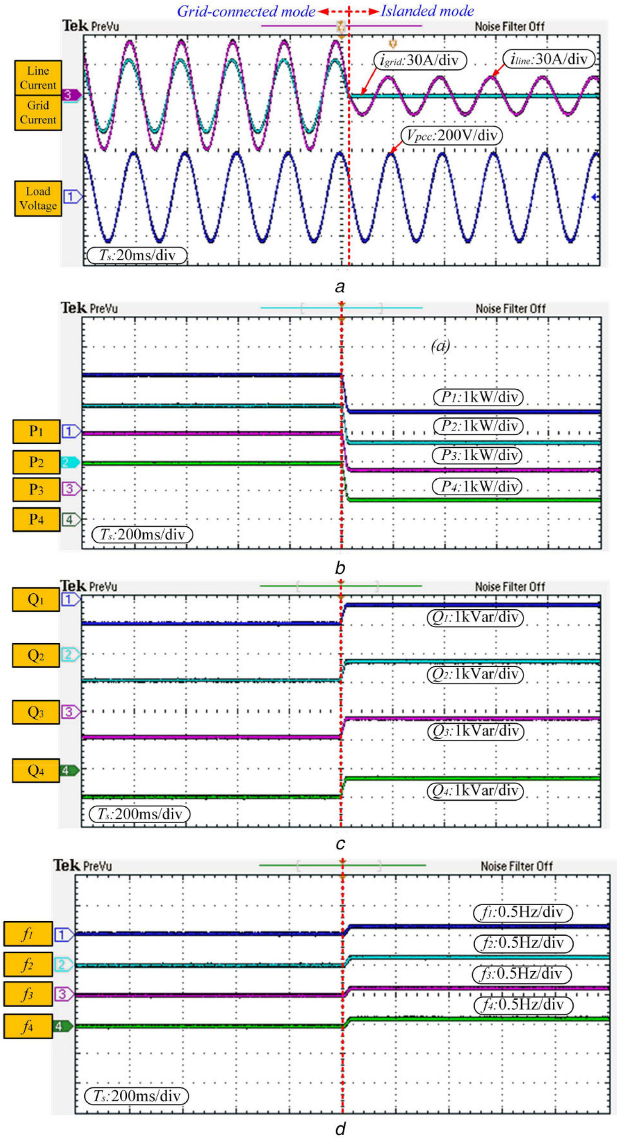

Fig. 23 *OPAL-RT-based real-time simulation tests of case 2*
(a) Voltage and current waveforms, ***(b)*** Active power, ***(c)*** Reactive power, ***(d)*** Frequency

6.2 Case 2: switch from grid-connected to islanded mode under RC loads

In this test, the proposed scheme is implemented under RC loads when the CMG operates from the grid-connected mode to islanded mode. The load power factor is set as 0.95. The waveforms of load voltage, line current and grid current are shown in Fig. 23*a*. The active power and reactive power allocations among DGs are depicted in Figs. 23*b* and *c*, respectively. As seen, the proposed scheme can inject the desired powers into the grid in grid-connected mode, and maintain the stable operation in islanded mode. The waveform of frequency is depicted in Fig. 23*d*, in which the system switches smoothly from the grid-connected mode to islanded mode.

From the OPAL-RT-based real-time simulation test results, the proposed unified decentralised control scheme is feasible for the grid-connected and islanded operation of CMG where the RC loads are fed.

7 Conclusion

This paper proposed a unified decentralised control strategy of CMG for both the grid-connected and islanded operation. The main results of this paper are summarised as follows: (i) seamless transition from the grid-connected mode to islanded mode is realised under both RL and RC loads; (ii) the CMG always holds a unique steady-state operation point; and (iii) the proposed scheme is a fully decentralised manner, as it is implemented only with the local information. In addition, the decentralised control scheme of multi-series networked topology will be studied in the future.

8 References

[1] Cho, C., Jeon, J., Kim, J., *et al.*: 'Active synchronizing control of a microgrid', *IEEE Trans. Power Electron.*, 2011, **26**, (12), pp. 3707–3719

[2] Assis, T. M. L., Taranto, G. N.: 'Automatic reconnection from intentional islanding based on remote sensing of voltage and frequency signals', *IEEE Trans. Smart Grid*, 2012, **3**, (4), pp. 1877–1884

[3] Wang, L., Zhang, D., Wang, Y., *et al.*: 'Power and voltage balance control of a novel three-phase solid-state transformer using multilevel cascaded H-bridge inverters for microgrid applications', *IEEE Trans. Power Electron.*, 2016, **31**, (4), pp. 3289–3301

[4] Karasani, R.R., Borghate, V.B., Meshram, P.M., *et al.*: 'A three-phase hybrid cascaded modular multilevel inverter for renewable energy environment', *IEEE Trans. Power Electron.*, 2017, **32**, (2), pp. 1070–1087

[5] Mortezaei, A., Simões, M. G., Bubshait, A. S., *et al.*: 'Multifunctional control strategy for asymmetrical cascaded H-bridge inverter in microgrid applications', *IEEE Trans. Ind. Appl.*, 2017, **53**, (2), pp. 1538–1551

[6] Li, L., Sun, Y., Han, H., *et al.*: 'Power factor angle consistency control for decentralized power sharing in cascaded-type microgrid', *IET Gener. Transm. Distrib.*, 2019, **13**, (6), pp. 850–857

[7] Lasseter, R.H.: 'Microgrids'. Proc. IEEE Power Engineering Soc. Winter Meeting, 2002, pp. 305–308

Q6 [8] Han, H., Hou, X., Yang, J., *et al.*: 'Review of power sharing control strategies for islanding operation of AC microgrids', *IEEE Trans. Smart Grid*, 2016, **7**, (1), pp. 200–215

[9] Li, L., Sun, Y., Liu, Z., *et al.*: 'A series-parallel PV-storage independent microgrid and its decentralized control', *Int. Trans. Electr. Energy Syst.*, 2019, **29**, (2), p. e2715

[10] Jiang, W., Xue, S., Zhang, L., *et al.*: 'Flexible power distribution control in an asymmetrical-cascaded-multilevel-converter-based hybrid energy storage system', *IEEE Trans. Ind. Electron.*, 2018, **65**, (8), pp. 6150–6159

[11] Zhang, L., Sun, K., Xing, Y., *et al.*: 'A modular grid-connected photovoltaic generation system based on DC bus', *IEEE Trans. Power Electron.*, 2011, **26**, (2), pp. 523–531

[12] Xiao, B., Hang, L., Mei, J., *et al.*: 'Modular cascaded H-bridge multilevel PV inverter with distributed MPPT for grid-connected applications', *IEEE Trans. Ind. Appl.*, 2015, **51**, (2), pp. 1722–1731

[13] Iman-Eini, H., Bacha, S., Frey, D.: 'Improved control algorithm for grid-connected cascaded H-bridge photovoltaic inverters under asymmetric operating conditions', *IET Power Electron.*, 2018, **11**, (3), pp. 407–415

[14] Jafarian, H., Cox, R., Enslin, J. H., *et al.*: 'Decentralized active and reactive power control for an AC-stacked PV inverter with single member phase compensation', *IEEE Trans. Ind. Appl.*, 2018, **54**, (1), pp. 345–355

[15] Jafarian, H., Bhowmik, S., Parkhideh, B.: 'Hybrid current-/voltage-mode control scheme for distributed AC-stacked PV inverter with low-bandwidth communication requirements', *IEEE Trans. Ind. Electron.*, 2018, **65**, (1), pp. 321–330

[16] Malinowski, M., Gopakumar, K., Rodriguez, J., *et al.*: 'A survey on cascaded multilevel inverters', *IEEE Trans. Ind. Electron.*, 2010, **57**, (7), pp. 2197–2206

[17] Rodriguez, J., Lai, J.S., Peng, F.Z.: 'Multilevel inverters: a survey of topologies, controls, and applications', *IEEE Trans. Ind. Electron.*, 2002, **49**, (4), pp. 724–738

[18] Jafarian, H., Kim, N., Parkhideh, B.: 'Decentralized control strategy for AC-stacked PV inverter architecture under grid background harmonics', *IEEE J. Emerg. Sel. Top. Power Electron.*, 2018, **6**, (1), pp. 84–93

[19] Guo, X., Zhou, J., He, R., *et al.*: 'Leakage current attenuation of a three-phase cascaded inverter for transformer less grid-connected PV systems', *IEEE Trans. Ind. Electron.*, 2018, **65**, (1), pp. 676–686

[20] Jiang, W., Huang, L., Zhang, L, *et al.*: 'Control of active power exchange with auxiliary power loop in a single-phase cascaded multilevel converter-based energy storage system', *IEEE Trans. Power Electron.*, 2017, **32**, (2), pp. 1518–1532

[21] Lamb, J., Mirafzal, B., Blaabjerg, F., *et al.*: 'PWM common mode reference generation for maximizing the linear modulation region of CHB converters in islanded microgrids', *IEEE Trans. Ind. Electron.*, 2018, **65**, (7), pp. 5250–5259

[22] Hamzeh, M., Ghazanfari, A., Mokhtari, H., *et al.*: 'Integrating hybrid power source into an islanded MV microgrid using CHB multilevel inverter under unbalanced and nonlinear load conditions', *IEEE Trans. Energy Convers.*, 2013, **28**, (3), pp. 643–651

[23] Yu, Y., Konstantinou, G., Hredzak, B., *et al.*: 'Power balance of cascaded H-bridge multilevel converters for large-scale photovoltaic integration', *IEEE Trans. Power Electron.*, 2016, **31**, (1), pp. 292–303

[24] Chatzinikolaou, E., Rogers, D. J.: 'A comparison of grid-connected battery energy storage system designs', *IEEE Trans. Power Electron.*, 2017, **32**, (9), pp. 6913–6923

[25] He, J., Li, Y., Wang, C., *et al.*: 'Hybrid microgrid with parallel- and series-connected microconverters', *IEEE Trans. Power Electron.*, 2018, **33**, (6), pp. 4817–4831

[26] Hou, X., Sun, Y., Han, H., *et al.*: 'A fully decentralized control of grid-connected cascaded inverters', *IEEE Trans. Sustain. Energy*, 2019, **10**, (1), pp. 315–317

[27] He, J., Li, Y., Liang, B., *et al.*: 'Inverse power factor droop control for decentralized power sharing in series-connected-microconverters-based islanding microgrids', *IEEE Trans. Ind. Electron.*, 2017, **64**, (9), pp. 7444–7454

[28] Sun, Y., Shi, G., Li, X., *et al.*: 'An f-P/Q droop control in cascaded-type microgrid', *IEEE Trans. Power Syst.*, 2018, **33**, (1), pp. 1136–1138

[29] Li, L., Sun, Y., Liu, Z., *et al.*: 'A decentralized control with unique equilibrium point for cascaded-type microgrid', *IEEE Trans. Sustain. Energy*, 2019, **10**, (1), pp. 324–326

[30] Hou, X., Sun, Y., Lu, J., *et al.*: 'Distributed hierarchical control of AC microgrid operating in grid-connected, islanded and their transition modes', *IEEE Access*, 2018, **6**, pp. 77388–77401

[31] Sun, Y., Zhong, C., Hou, X., *et al.*: 'Distributed cooperative synchronization strategy for multi-bus microgrids', *Int. J. Electr. Power Energy Syst.*, 2017, **86**, pp. 18–28

[32] Dragicevic, T., Wu, D., Shafiee, Q., *et al.*: 'Distributed and decentralized control architectures for converter-interfaced microgrids', *Chinese J. Electr. Eng.*, 2017, **3**, (2), pp. 41–52

[33] Li, L., Ye, H., Sun, Y., *et al.*: 'A communication-free economical-sharing scheme for cascaded-type microgrids', *Int. J. Electr. Power Energy Syst.*, 2019, **104**, pp. 1–9

[34] Guerrero, J. M., Chandorkar, M., Lee, T., *et al.*: 'Advanced control architectures for intelligent microgrids – part i: decentralized and hierarchical control', *IEEE Trans. Ind. Electron.*, 2013, **60**, (4), pp. 1254–1262

[35] Han, Y., Li, H., Shen, P., *et al.*: 'Review of active and reactive power sharing strategies in hierarchical controlled microgrids', *IEEE Trans. Power Electron.*, 2017, **32**, (3), pp. 2427–2451

[36] Simpson-Porco, J.W., Dörfler, F., Bullo, F.: 'Synchronization and power sharing for droop-controlled inverters in islanded microgrids', *Automatica*, 2013, **49**, (9), pp. 2603–2611

[37] Maharjan, L., Yamagishi, T., Akagi, H., *et al.*: 'Fault-tolerant operation of a battery-energy-storage system based on a multilevel cascade PWM converter with star configuration', *IEEE Trans. Power Electron.*, 2010, **25**, (9), pp. 2386–2396